NASA CR-66973

THREE-DIMENSIONAL PHOTOELASTIC EVALUATION OF WIRE REINFORCED FLEXIBLE WINDOWS

by

R. C. Sampson

September 1969

University of Washington
Department of Aeronautics and Astronautics
Seattle, Washington 98105

Prepared under Grant No. NGR 48-002-003 from
the National Aeronautics and Space Administration

ABSTRACT

Models of reinforced flexible windows for inflatable spacecraft were constructed using steel reinforcing rods in an epoxy matrix. The stress state in the matrix due to combined thermal shrinkage and lateral pressure was determined by the frozen-stress technique of photoelasticity. The correlation with the prototype is also presented.

TABLE OF CONTENTS

List of Figures

TABLE OF CONTENTS (CON'T.)

INTRODUCTION

The concept of manned inflatable space structures calls for the incorporation of observation windows of good optical clarity and having flexibility compatible with the folded condition of the main structure. Developmental testing and evaluation of candidate materials and window construction schemes have indicated that a satisfactory construction is achieved by an orthogonal network of stranded steel cable embedded in a matrix of urethane rubber.[1] A thin film of silicone rubber was applied to the surfaces in order to improve surface smoothness and optical quality.

In the experiments reported here, the primary objective was to determine the stress state in the composite window structure imposed by typical loading conditions encountered in the prototype window. Adverse stress conditions might have deleterious effects not only on the structural integrity, but also the optical quality of the window. Local deformations of the surfaces are also of particular interest because of the extremely adverse effect on the visual quality of the window caused by local "dimpling."

The experimental techniques for photoelastic analysis of composite structures have been developed to the point where this investigation is feasible. As a matter of general interest, Appendix A was prepared giving a cursory review of some of the chief published papers in the field of photoelastic

analysis of composites. Applications have varied from super-scale model studies of embedded inclusion microstructure stresses to subscale models of large solid rocket motor assemblies.

STRUCTURAL TEST CONSIDERATIONS

Since the model studies should represent the prototype window structure as closely as possible, careful consideration was given as to the best means of simulating actual conditions. It was concluded that the principal loads are those caused by: (a) differential thermal contraction of the rubber and steel constituents of the composite window, (b) stresses induced by internal pressure acting on the inflated structure,and (c) stresses induced by general curvature of the window. It was further concluded that each "cell" of the window is virtually identical to any other, and that a model incorporating very many of these identical cells would not be necessary. Instead, the test concept was to simulate only a few neighboring cells subjected to typical loading conditions. Analysis of one of these cells would then provide all the needed information on stress in a typical cell under a combination of loading conditions.

From an elementary strength of materials analysis, it is clear that the steel reinforcement cable sustains nearly the entire load that is induced by pressure. The transparent rubber merely acts to retain the gases within the structure

and to transmit the pressure thrust to the steel cables. In doing this, large tension is introduced in the cables and the pressure thrust on the rubber cells tends to bulge them outward. This is the condition that was planned in devising the model test fixture. A means for providing, simultaneously, high tensile stress in the reinforcement and uniform lateral pressure on the simulated rubber matrix was devised. In conjunction with this, a substantial differential thermal shrinkage effect was also introduced in the model. As previously mentioned, this also has its counterpart in the prototype operational environment. Figure 1 shows schematically, the effective boundary conditions prevailing in a typical cell. Steel cables under tension F provide an essentially rigid boundary to the D $\times$ D inch cell. The rubber, of thickness h , is subjected to pressure p . The expansion coefficients of steel and rubber are α_s and α_r respectively, while the initial and final temperatures of the composite are T_1 and T_2 respectively. The elastic moduli of the steel and rubber constituents are E_s and E_r respectively. A general curvature $1/\rho$ is inevitably introduced by the application of lateral pressure, in addition to the local curvatures resulting from individual cell wall bulges.

MODEL TEST TECHNIQUES

Ideally, the test objectives should be accomplished by preparing two models, one to be subjected to lateral pressure loading and the other to thermal shrinkage effects. At the present state of the art, shrinkage effects cannot be entirely eliminated in composite frozen-stress models made from dissimilar materials. Thus, the pressure loaded model must also contain shrinkage effects. The two-model method for separating these stress systems has been effectively employed in other investigations [2] , but considerable time is required to accomplish the tedious stress-separation procedures that are required and the technique was not used in this study. Instead, this analysis makes use of only one model which represents the prototype operating at one particular pressure, p , and one particular value of free thermal shrinkage stress,

$$E\Delta = E(\alpha_r - \alpha_s)(T_1 - T_2)$$

The two operating conditions are not separately distinguishable in this case.

Conventional "Frozen-Stress"

The pressure stress effects are imposed on the model by the well-known "stress-freezing" technique.[3] Essentially,

the photoelastic model is heated to its "critical" temperature where it assumes a rubbery state. Pressure is applied at that temperature, inducing deformations in the model. As the model is slowly cooled, it achieves its original hard, glass-like character but the deformations imposed at the higher temperature remain. The deformations (and the photoelastic effect) are thus fixed or "frozen" into the model. Unloading, or even cutting the model in sections, does not alter the "frozen" patterns of stress. The familiar stress-optic law applies to the frozen-stress photoelastic pattern equally as well as to two-dimensional stress states in models tested at room temperature:

$$\sigma_1 - \sigma_2 = \frac{nf}{t} = Nf \quad , \tag{1}$$

where

$\sigma_1 - \sigma_2$ = the difference of principal stresses in the plane of the frozen-stress slice in psi,

n = the observed slice isochromatic fringe order,

t = the slice thickness in inches,

f = the model material frozen stress-fringe value in psi-inches per fringe,

N = the fringe order per inch of slice thickness in fringes per inch.

At free boundaries, one of these principal stresses is zero

and the other component is then determined directly by equation (1). Stresses at interior points may also be determined, but other information must be provided, such as the isoclinic (stress-direction) angle. Then, for example, the differential equations of equilibrium can be employed in a numerical integration procedure to achieve separation of the two principal stresses (see Ref.[3],pp. 235-247). Maximum shear stresses, on the other hand, are obtained directly from the isochromatic pattern since, with equation (1),

$$\tau_{max} = \frac{\sigma_1 - \sigma_2}{2} = \frac{nf}{2t} \quad . \tag{2}$$

Thermal Shrinkage Stress Freezing

Composite structures of dissimilar materials characteristically develop differential shrinkage stresses upon change of temperature. Until recently, problems of this nature were not susceptible to photoelastic analysis [4]. In thermal shrinkage stress freezing, a composite model is prepared in which the materials are free of differential thermal effects at (or near to) the "critical" or rubber-like temperature of the photoelastic polymer component. Then, on cooling, differential contraction induces progressively larger forces of interaction (stress) between the two constituents. The rigid component (steel) has no appreciable strain induced in it,

and the polymer must then furnish all the compliance necessary to accommodate these forces. The forces become progressively larger as the assembly cools, and the polymer is also progressively hardening and becoming less susceptible to "freezing" of stress or deformation. Thus, at some point in cooling the polymer ceases to develop further frozen birefringence, but continues to develop this effect in that part of its molecular structure characterized as "glassy." When the model is cooled and subsequently sliced, removing the constraints imposed on the plastic, the birefringence stored in the "glassy" structure disappears and only the "frozen" birefringence accumulated in the "rubbery" molecular structure remains. Obviously, this type of stress freezing is more complex than the first. Nevertheless, the ultimate result is the same and equation (1) also expresses the proper relationship between thermal shrinkage stress and the observed fringe order. Equation (1), however, does not provide the needed relationship between fringe order and the thermal shrinkage parameter of the test, Δ . Reference [4] describes the special calibration procedures needed to insure quantitative accuracy of data presented in terms of stress difference per unit reference shrinkage stress:

$$\frac{(\sigma_1-\sigma_2)}{E\Delta} = \frac{C_1 N}{N_1} \quad , \tag{3}$$

where

$E\Delta$ = the reference thermal shrinkage stress,

C_1 = a constant associated with the test calibration specimen configuration,

N_1 = the calibration specimen fringe order in a thickness of one inch in fringes per inch,

N = the model slice observed fringe order in a slice one inch thick in fringes per inch.

Since equations (1) and (3) both apply to the thermal shrinkage frozen-stress pattern, we combine them to solve for the effective shrinkage stress pertaining to the test:

$$E\Delta = \frac{N_1 f}{C_1} \quad . \tag{4}$$

Thus, the reference thermal shrinkage stress in effect during the model test is determined. The model shrinkage test results pertain directly to the prototype operating at the same reference stress level, i.e.,

$$(E\Delta)_{\text{prototype}} = (E\Delta)_{\text{model test}} \quad . \tag{5}$$

The effective temperature drop of the prototype, for which the model shrinkage stresses directly correspond, is determined from the definition of $E\Delta$ and employing equation (4):

$$(T_1 - T_2) = \frac{N_1 f}{C_1 E_r (\alpha_r - \alpha_s)} \quad , \tag{6}$$

where E_r , α_r and α_s now pertain to the prototype window.

PREPARING THE MODELS

A model comprising a 3 × 3 array of cells was designed to represent a 5× scale model of a prototype window in which the cell size D = ½ inch, the steel cable diameter d = .025 inches, and the window thickness h = 0.10 and 0.15 inches respectively in two consecutive models. The casting mold designed for production of these models is shown in Figure 2. Drill rod with threaded ends represents the reinforcing cable and tensions near the limit load for the threaded sections are applied by nuts supported by the side rails. Two sets of side rails were prepared to suit the two models having different thickness. The crossed reinforcing rods are arranged symmetrically about the middle plane of the window, and the two sets of rods are separated at their crossover points by a nominal 1/32 inch. Figure 3 is a photograph of the mold, assembled and ready for casting the photoelastic resin. In preparation for casting, the reinforcing wires were thoroughly cleaned and degreased to promote the best possible bond with the resin. Other parts of the mold were treated with a mold release agent to prevent adhesion.

A resin mixture of the following constituents was mixed thoroughly (see Ref. [4] for a detailed description of this photoelastic material):

50 pbw* Bakelite Resin** ERL 2774

50 pbw Bakelite Resin ERL 2795

25 pbw Bakelite Hardener ZZL 0803

The liquid resin was poured into the mold after thoroughly mixing and degassing to eliminate air bubbles. A slow curing process requiring gradually increased temperatures up to 75°C was then applied. This process requires several days and at the end it was slowly cooled to room temperature.

Two models were prepared in this manner, the first, Model A, having a thickness of 0.50 inches. Model B was 0.75 inches thick.

TEST PROCEDURES

The purpose of the test is to "freeze" the photoelastic stress patterns in the cured model while applying load conditions closely simulating the conditions prevailing on a prototype window. To accomplish this, it was required to apply lateral pressure to the model while at the same time, strong tensile stress was applied to the reinforcing wires. This is the condition prevailing in the prototype window of the inflated structure. Accordingly, the model, cured in place in the casting mold of Figures 2 and 3, was replaced in that mold.

---

* parts by weight
**products of the Union Carbide Corp.

The mold serves as a testing frame for application of strong reinforcement tensions by means of nuts torqued on the threaded ends of the rods protruding through the sides of the mold side rails. A pressure tap was installed in the bottom plate of the mold and a silicone rubber sealant was applied near the periphery at the bottom surface of the model, in order to contain the pressure. Nitrogen gas pressure at 7.00 psig was introduced in this confined space and the model was heated to 75°C for several hours, then slowly cooled to room temperature while holding the pressure constant. In this manner, stresses due to both lateral pressure and differential thermal shrinkage were "frozen" in the model. A line pressure regulator and a mercury manometer were used to maintain and measure the applied pressure. Both models were frozen-stressed in this same manner.

After stress-freezing, the model was removed from the test fixture and a set of slices removed for analysis. Slices were rough cut with a bandsaw, then machined uniformly smooth on a surface grinder in a coolant bath. Positions of the slices are indicated in Figure 4.

Prior to the removal of any slices, the deformation contours of the top surface of the model along the x and y axes (Figure 1) were explored using a vernier height gage. Thus, the curve of deflection versus distance from the plate edges was determined.

Table I gives the principal data on the model, material, and test conditions. The values of E, ν and f for stress freezing of this material were established in a number of previous experimental tests. The reference thermal stress $E\Delta$ was computed from equation (4) in which the fringe order N_1 was obtained from a calibration specimen that was cast and cured in company with Model A. This was a circular cylindrical specimen 6 inches long and with $2b = 7/8$ inch in diameter, with a centrally embedded steel mandrel, $2a = 3/16$ inch diameter, strongly bonded to the resin. This produces complete elastic restraint of all differential thermal shrinkage at the interface, in both the tangential ($\epsilon_\theta = \Delta$) and longitudinal ($\epsilon_z = \Delta$) directions. Under these boundary conditions, the basic Lamé cylinder equations [5] provide the basis for the following solution at the interface ($r = a$) :

$$\sigma_\theta = \sigma_z = \frac{(1+b^2/a^2)\ E\Delta}{(b^2/a^2) + 1-2\nu} \quad , \tag{7}$$

$$\sigma_r = \frac{(1-b^2/a^2)\ E\Delta}{(b^2/a^2) + 1-2\nu} \quad , \tag{8}$$

$$\sigma_\theta - \sigma_r = \sigma_z - \sigma_r = \frac{2(b^2/a^2)\ E\Delta}{(b^2/a^2) + 1-2\nu} \tag{9}$$

Note that from equations (3) and (9) the value of the calibration specimen coefficient is (since in this case $N = N_1$)

$$C_1 = \frac{\sigma_\theta - \sigma_r}{E\Delta_{cal.}} = \frac{2\, b^2/a^2}{(b^2/a^2) + 1-2\nu} \quad . \qquad (10)$$

Thus, C_1 has the value very close to 2 . The value of $E\Delta$ was then found from equation (4) ,

$$E\Delta = \frac{N_1 f}{C_1} = \frac{(11.13)(1.40)}{2} = 7.90 \text{ psi} \quad ,$$

in which the value $N_1 = 11.13$ was measured from a transverse slice taken from the calibration cylinder.

TABLE I

Model Materials Properties
and Test Conditions

		Model Test	A	B
h	=	thickness, inches	0.50	0.72
p	=	applied pressure, psig	7.00	7.00
E	=	effective elastic modulus, psi	1800	1800
f	=	frozen-stress fringe value, $\frac{\text{psi - inches}}{\text{fringe}}$	1.40	1.40
ν	=	frozen-stress Poisson's Ratio	0.49	0.49
$E\Delta$	=	reference thermal shrinkage frozen-stress, psi	7.90	7.90

DEFLECTIONS

Local deflections of the window within the boundaries of each cell are important because of the adverse effect on the visual or photographic resolution of subjects viewed through the window. This pattern of local curvature will produce local deviations of the paths of transmitted light rays and the eye will be unable to accommodate these aberrations. Thus, the image is degraded whether the viewer places himself near or at some distance, from the window. It is important then to minimize these local deflections. The results reported in Reference [1] indicate that better window visibility is achieved when the cell size is large, so that the eye placed close to the window can view the subject by light rays passing through a single cell. In that way, the psychologically distracting and optically diffracting effects of the reinforcement wires are minimized. While this indicates that the cell size should be as large as possible, this size will be limited by the standards of acceptable stress and curvature within the cell. The test results presented here will provide a basis for judging suitable limits on size.

The deflection curve from the edge to the center of window for Model A is shown in Figure 5. The bulging of the plate as a whole under lateral pressure tends to mask the local cell deflection, and the dashed curve of apparent plate deflection has been blended in as an estimated basis for comparison.

A local deflection in the central cell of about .015 inches is indicated. The prototype deflection is related to that in the model by the relation

$$\left(\frac{pL}{yE}\right)_{\text{model}} = \left(\frac{pL}{yE}\right)_{\text{prototype}} , \qquad (11)$$

where

p = the lateral pressure in psig,

L = a characteristic window cell dimension in inches,

E = the matrix elastic modulus in psi,

y = the local deflection of the cell.

Taking the model values of p , L and E as 7.0 psi, 2.50 inches (cell size), and 1800 psi respectively, we obtain for corresponding prototype parameters of 7.0 psi, 0.50 inches and an estimated 600 psi, a cell deflection of

$$y_p = \frac{E_m}{E_p} \times \frac{p_p}{p_m} \times \frac{L_p}{L_m} \times y_m ,$$

$$= \frac{1800}{600} \times \frac{7}{7} \times \frac{0.50}{2.50} \times .015 , \qquad (12)$$

$$= .009 \text{ inches}$$

The prototype cell size corresponding to this result is 1/2 inch square by 0.10 inches thick.

Similarly, Figure 6 shows the deflection curve for Model B which was tested under nominally the same conditions except that the thickness was 0.72 inches. Here the local cell deflection was approximately one-half that observed in Model A. The corresponding prototype deflection is

$$y_p = \frac{1800}{600} \times \frac{7}{7} \times \frac{0.50}{2.50} \times .006$$

$$= .0036 \text{ inches} \quad ,$$

where the corresponding prototype cell size is again 1/2 inch square,but 0.144 inches thick. Since the deflections of the model as a whole cannot be accurately separated from the much smaller individual cell deflections, the maximum local cell deflections indicated in Figures 5 and 6 are probably not very accurate,but are sufficient for purposes of illustrating the effect of a change of window thickness. The approximate overall radii of curvature at the middle of the frozen-stressed window Models A and B were 75 inches and 58 inches respectively. In spite of its greater thickness and rigidity, more general bending was apparently induced in Model B under the same lateral pressure. It is therefore concluded that the effective edge constraints applied to the two models were not identical,and that consequently it will not be possible to make direct comparisons between the two sets of test results.

BOUNDARY STRESS DISTRIBUTIONS

Model A

Frozen-stress slices removed from Model A, as indicated by the sketch in Figure 4, are shown in Figure 7. Isochromatic fringes for both light and dark fields are shown and the fringe order n is noted at some locations. Interpretation of this data was accomplished by equation (1), with $f = 1.40$ psi inches per fringe. The slice thicknesses t were uniformly 0.150 inches. Boundary stresses were readily accomplished in that manner as well as the principal stress differences at interior points. Figure 8 shows the traverse of $(\sigma_1 - \sigma_2)$ along the principal section taken at the central point of Model A, in slice number 1. Differences between the observed and the interpolated data noted there are due to the absorption of water vapor at the slice boundaries. This introduces an extraneous stress and fringe order that must be compensated in order to avoid serious error in the results. The data indicate that this effect is equivalent to about 10 psi compressive stress, and this correction was applied to all boundary data. Note in Figure 8 that the neutral axis is located at $z/h = 0.23$ from the pressurized surface, indicating a substantial membrane tension as well as bending at that section. Variations of boundary stress along slice number 1 are shown in Figure 9. Minimum tension is at the central point on the upper boundary

and peak tensions occur on the pressurized surface also, directly beneath the reinforcing wires. Similar data for slice number 2 is shown in Figure 10, where the central point of the model is located just to the left of the slice sawcut on the left. It will be seen that the pattern of stresses is much the same in slices number 9 and 10 but that the stress peaks are not identical. Boundary stress peaks of comparable magnitude were not found in slice number 4 since the reinforcing rod completely dominates the deformation in that plane.

Model B

The isochromatic patterns in slices 1 and 2 taken from Model B are shown in Figure 11. The interpretation procedures employed here were identical to those described for Model A, and the boundary stress distribution for the principal slice, slice number 1, is shown in Figure 12. Comparison of Figure 12 to Figure 9 clearly shows that there is much less local bending effect in Model B in comparison to the overall bending effect. For example, there is no reversal of stress from tension to bending along either boundary of the slice in Model B, in contrast to Model A. Nevertheless, the maximum stress in Model B is, as expected, lower than in Model A on account of the greater thickness of the Model B.

RUBBER-STEEL INTERFACE STRESS CONCENTRATIONS

There is an obvious concentration of stress in the rubber matrix surrounding the reinforcing rods, as evidenced by the high fringe gradients seen in Figures 7 and 11. An evaluation of this interior stress condition was undertaken in order to identify the nature and magnitude of the local effects. The section selected for examination is that in slice number 1, Model A, as seen in the upper photograph of Figure 7. The section through the left-hand reinforcing rod was selected. A 10X photograph of this section is shown in Figure 13, where the lower surface is the pressurized face of the model.

In order to separate stresses, a numerical integration of the equation of equilibrium was performed along the section [3]. This required first the measurement of isoclinic angles θ as well as fringe order n all along the section. These data were readily obtained at 10X magnification in a contour projector-polariscope. In addition to the normal stresses in the matrix of the section, the shear stresses around the circular interface at the reinforcing rod were also determined from the relation

$$\tau_{xy} = \frac{\sigma_1 - \sigma_2}{2} \sin 2\theta \quad .$$

The normal stress separation method was that of Filon's transformation of the equilibrium equations in two-dimensions.

It was assumed that the section of interest is a section of symmetry and that all the data relevant to the equilibrium of an element is contained in the plane of the model slices. Under these restrictions, the equation to be evaluated is

$$\sigma_x = \sigma_{x,0} - \sum_{0}^{i} (\sigma_1 - \sigma_2) \frac{\Delta\theta}{\Delta y} \Delta x \quad .$$

Normal stresses obtained upon evaluating this equation are plotted in Figure 14. It will be noted that the most severe interface stress condition is a large compressive stress normal to the reinforcing rod. Diametrically opposite these is a normal tensile stress of somewhat smaller magnitude. These peak stresses do not exceed those previously found on the free surfaces of the rubber matrix. These local stresses are apparently the principal reaction stresses to the pressure thrust exerted on the rubber cells and reacted by the reinforcing rods. It should be noted that thermal shrinkage stresses also contribute to the total at the interface.

Shear stresses varying around the circumference of the reinforcing rod are shown in Figure 15. Again, the major influence in the build-up on shear stress seems to be the result of the transfer of pressure thrust from the rubber cell to the steel reinforcing rod.

In summary, the concentrations of stress in the rubber surrounding the steel rods includes substantial components of normal end shear stress, but the magnitudes are not severe in

comparison with the observed maximum free boundary stresses. Of course, if the rubber-steel bond strength is much less than the strength of the rubber itself, then the interface would constitute the weakest point of the composite structure.

PROTOTYPE STRESSES

As mentioned previously, the frozen-stress observed in the model is the result of two combined loads (thermal shrinkage and lateral pressure) and the restraint conditions applied at the edge of the model. Each model test result must be considered separately since direct comparisons will be made inaccurate due to unavoidable differences in edge constraint in the two model tests. Nevertheless, each model test is typical of a condition that may occur in the prototype.

In order to relate the large scale model test to the appropriate environmental condition of the prototype window, model-prototype similarity requirements must be considered for the three effects noted in the window model, i.e.,

(a) thermal stress induced by differential thermal shrinkage, Δ , between the reinforcement and the matrix,

(b) local bending stress in the cell induced by lateral pressure, p ,

(c) overall bending of the model to a radius of curvature ρ by the combined action of the lateral pressure and the edge restraints applied on the model.

Geometric similarity of the model and the prototype is assured

in all cases. It remains to determine the temperature change, lateral pressure, and window curvature applied to the prototype that will produce the same stresses as were noted in the model.

In case (a) above, the relationship between the prototype and its scale model is

$$\left(\frac{\sigma}{E\Delta}\right)_{model} = \left(\frac{\sigma}{E\Delta}\right)_{prototype} ,$$

from which the conclusion is reached that the quantity $E\Delta$ must be the same in both. From Table I, $E\Delta$ is 7.90 psi. Recalling that

$$E\Delta = 7.90 \text{ psi} = (\alpha_r - \alpha_w)(T_1 - T_2)E ,$$

and taking $(\alpha_r - \alpha_w) = 100 \times 10^{-6}/\text{deg.F}$ and $E = 600$ psi* , we get $(T_1 - T_2) = 7.90 \times 10^6/(600 \times 100) = 132^\circ\text{F}$. Taking the initial temperature $T_1 = 75^\circ\text{F}$, then the temperature corresponding to the stressed window condition is -57°F.

For case (b) above, the relationship between the prototype and its scale model is

$$\left(\frac{\sigma}{p}\right)_{model} = \left(\frac{\sigma}{p}\right)_{prototype}$$

*Lacking specific data, the elastic modulus of the rubber matrix and its expansion coefficient were estimated.

Thus, the model test pressure is the same that must be imposed on the prototype in order to produce the same stresses; in this case, $p = 7.00$ psig for both Models A and B and their respective prototypes.

In case (c) above, the general bending produces a radius of curvature ρ that has a functional relationship to the window parameters as follows:

$$\frac{1}{\rho} \sim \frac{M}{EI} \sim \frac{\sigma}{EL} \quad ,$$

where L is a characteristic dimension of the window, say the cell dimension. Then

$$\left(\frac{EL}{\rho}\right)_{\text{model}} = \left(\frac{EL}{\rho}\right)_{\text{prototype}} \quad .$$

Again taking $E = 600$ psi and with the model scale factor (L model $\div$ L prototype) equal to 5, the appropriate prototype radius of curvature corresponding to Model test A ($\rho_{\text{mod.A}} = 75$ in.) is

$$\rho_{\text{prot.}} = \frac{(EL)_{\text{prot.}}}{(EL)_{\text{mod.}}} \quad \rho_{\text{mod.}} = \frac{(600)(1)(75)}{(1800)(5)} \quad ,$$

$$\rho_{\text{prot.}} = 5 \text{ inches} \quad .$$

For test B, the radius of curvature observed in the model was 58 inches and the equivalent prototype radius is then

$$\rho_{prot.} = \frac{(600)(1)(58)}{(1800)(5)} = 3.87 \text{ inches} \quad .$$

These prototype conditions are summarized in Table II. Under all these conditions applied simultaneously, the stresses in the prototype can be taken the same as those values previously shown in the model test data. These conditions are inseparable as there is insufficient data available to predict the stresses resulting from a different combination of loads.

TABLE II

Prototype Conditions Required to Produce the Same Matrix Stresses as Observed in the Model

	Test A	Test B
Temperature change, $^{\circ}F$	-132	-132
Lateral pressure, psig	7.0	7.0
Window radius of curvature, inches	5.0	3.87

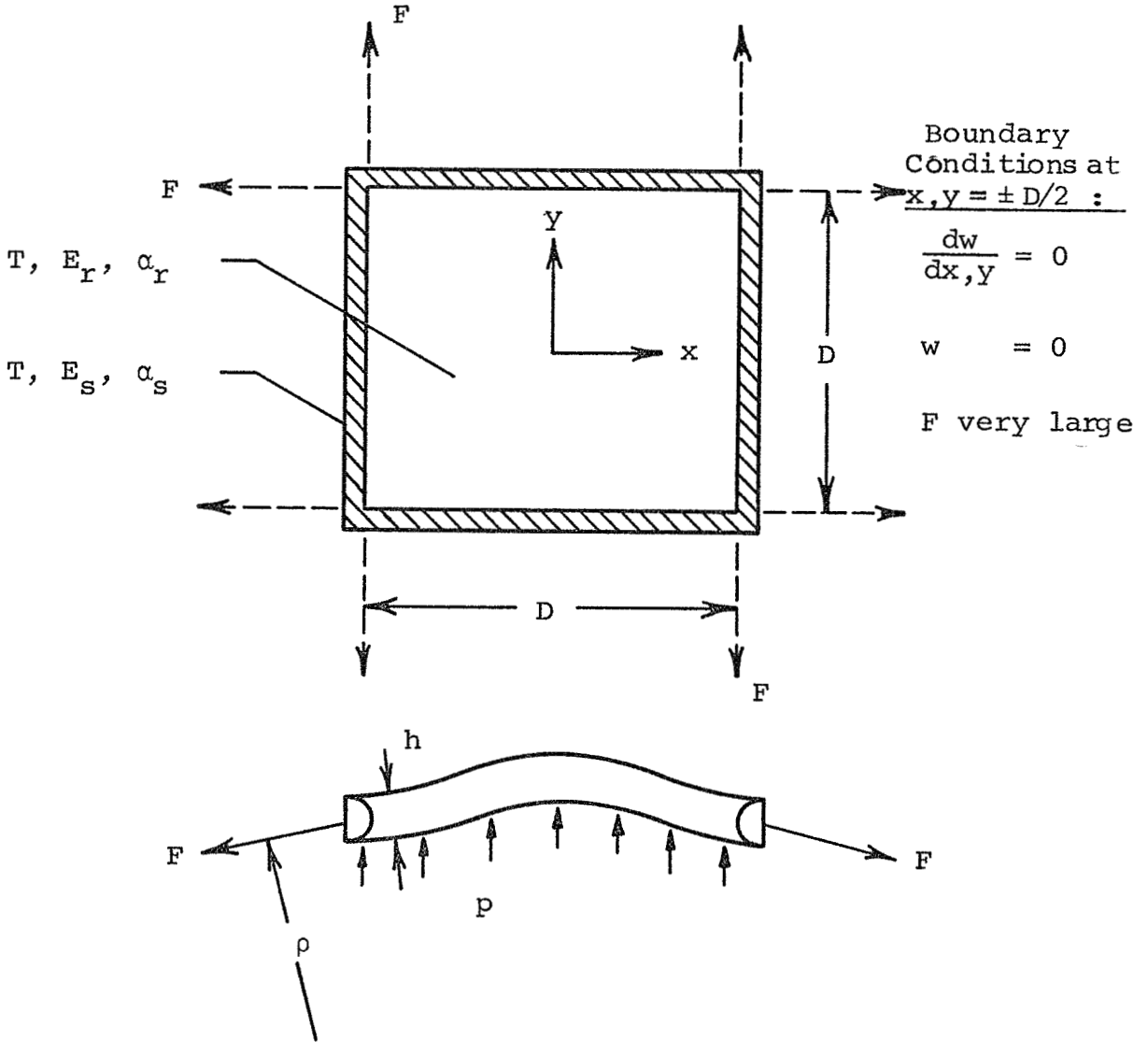

Figure 1. Conditions on Single Window Cell

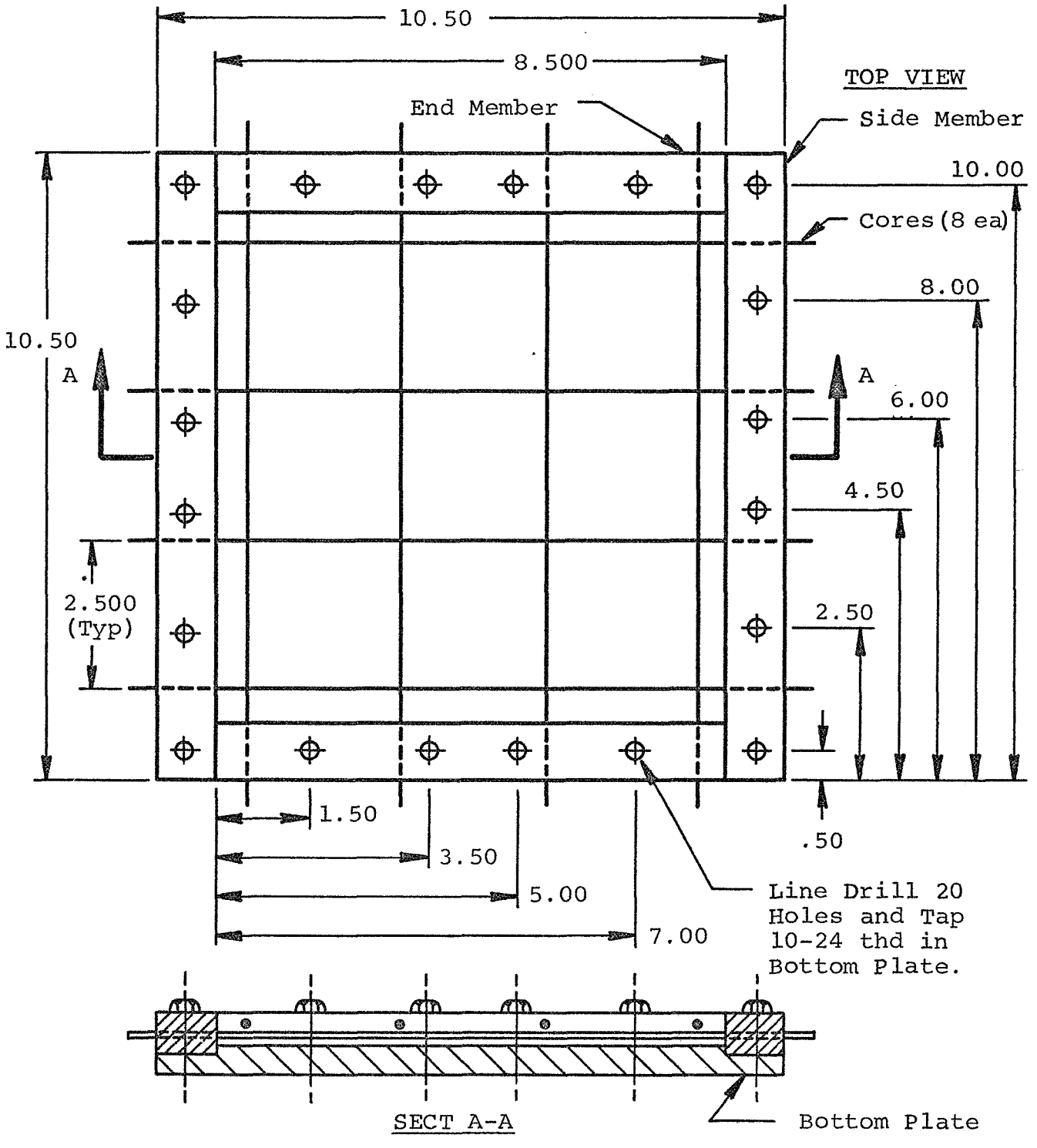

Figure 2. Window Model Casting Mold Assembly

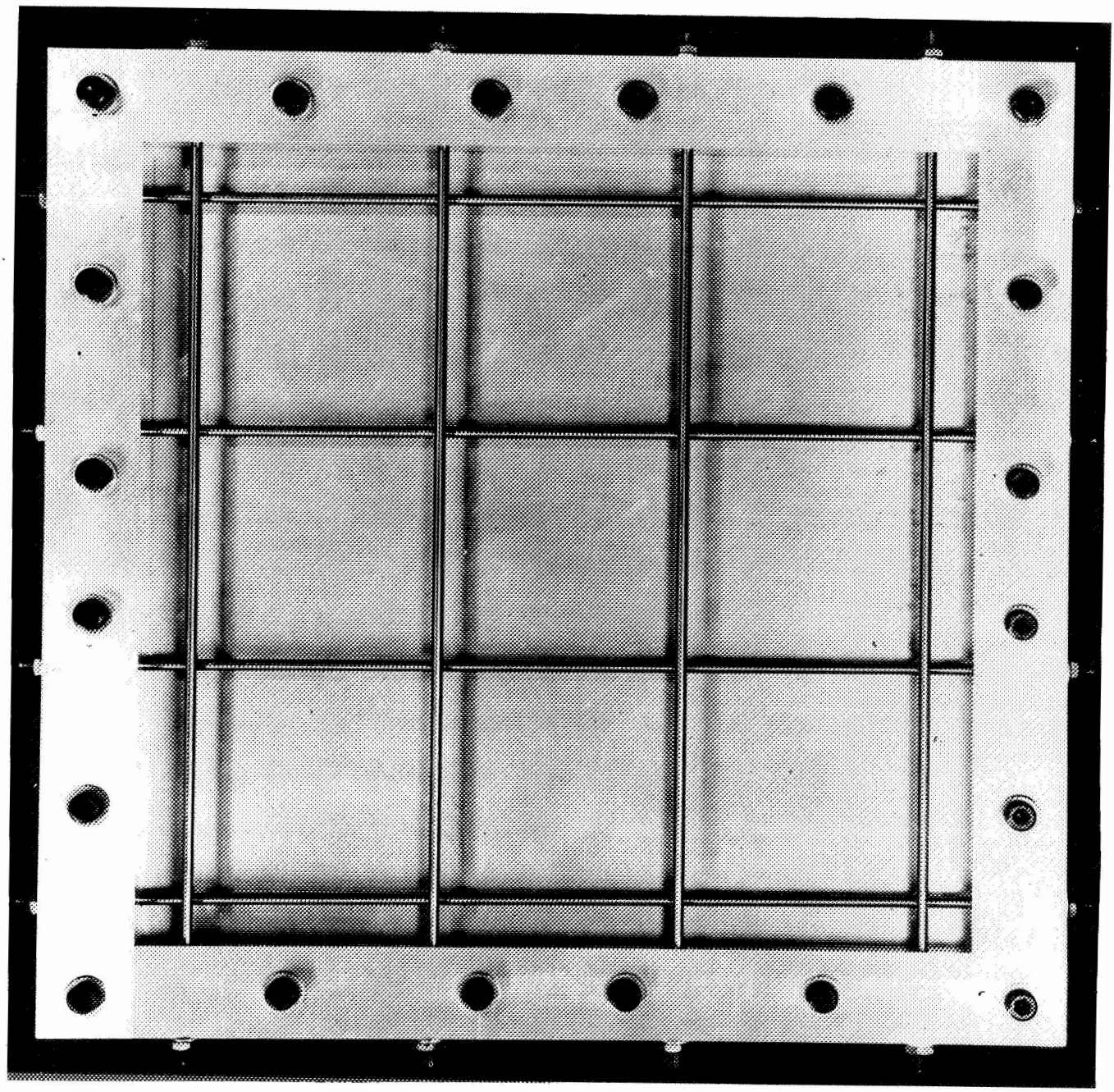

Figure 3. Casting Mold

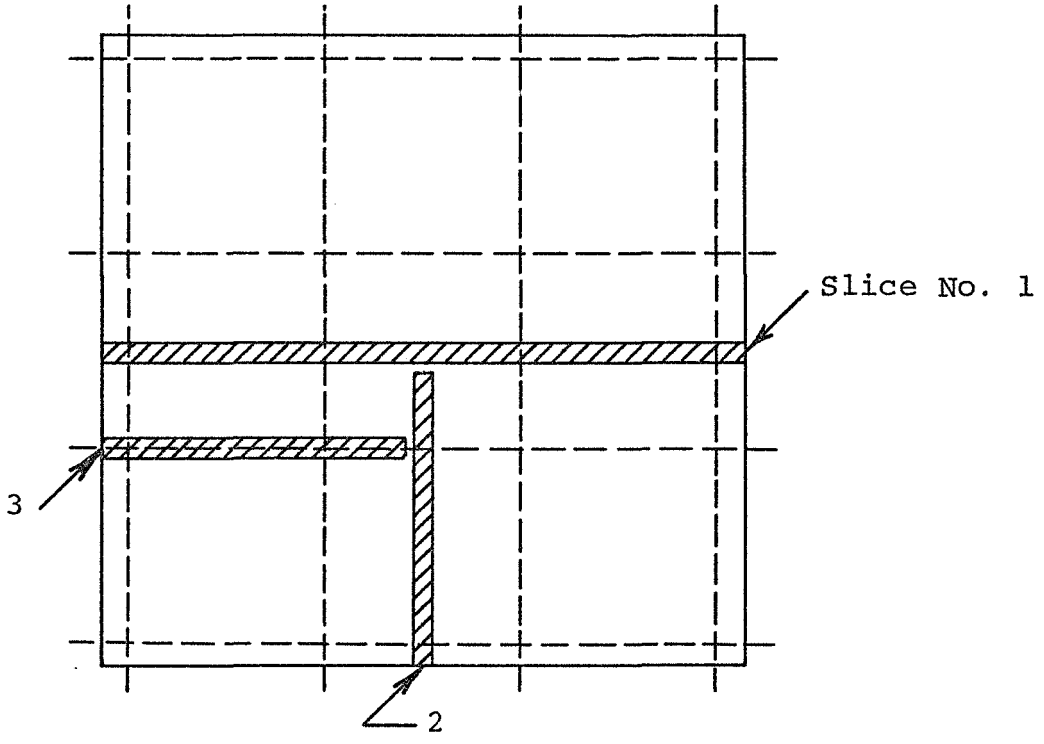

Figure 4. Window Model Slice Plan

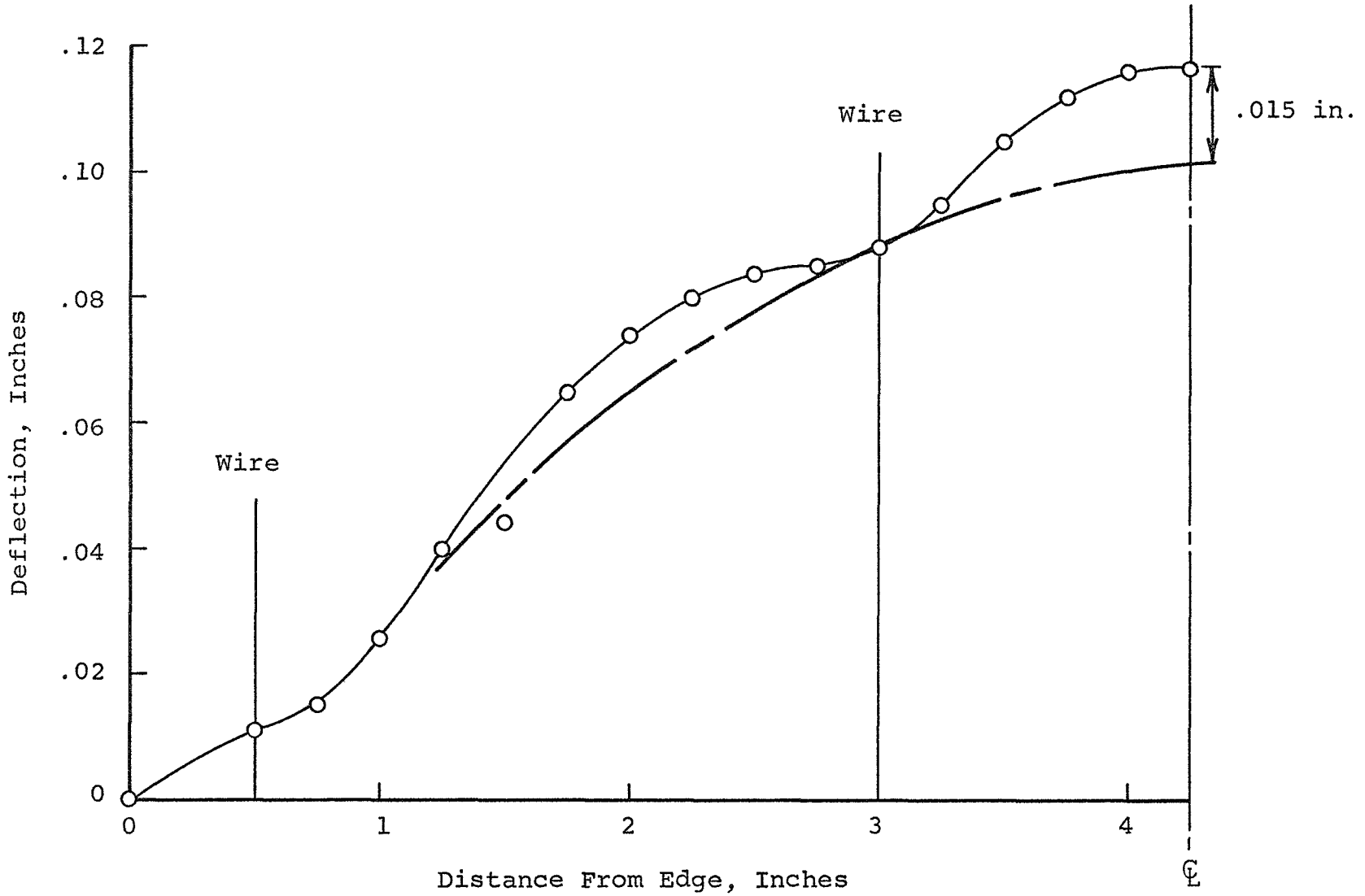

Figure 5. Deflection of Window Model, Test A

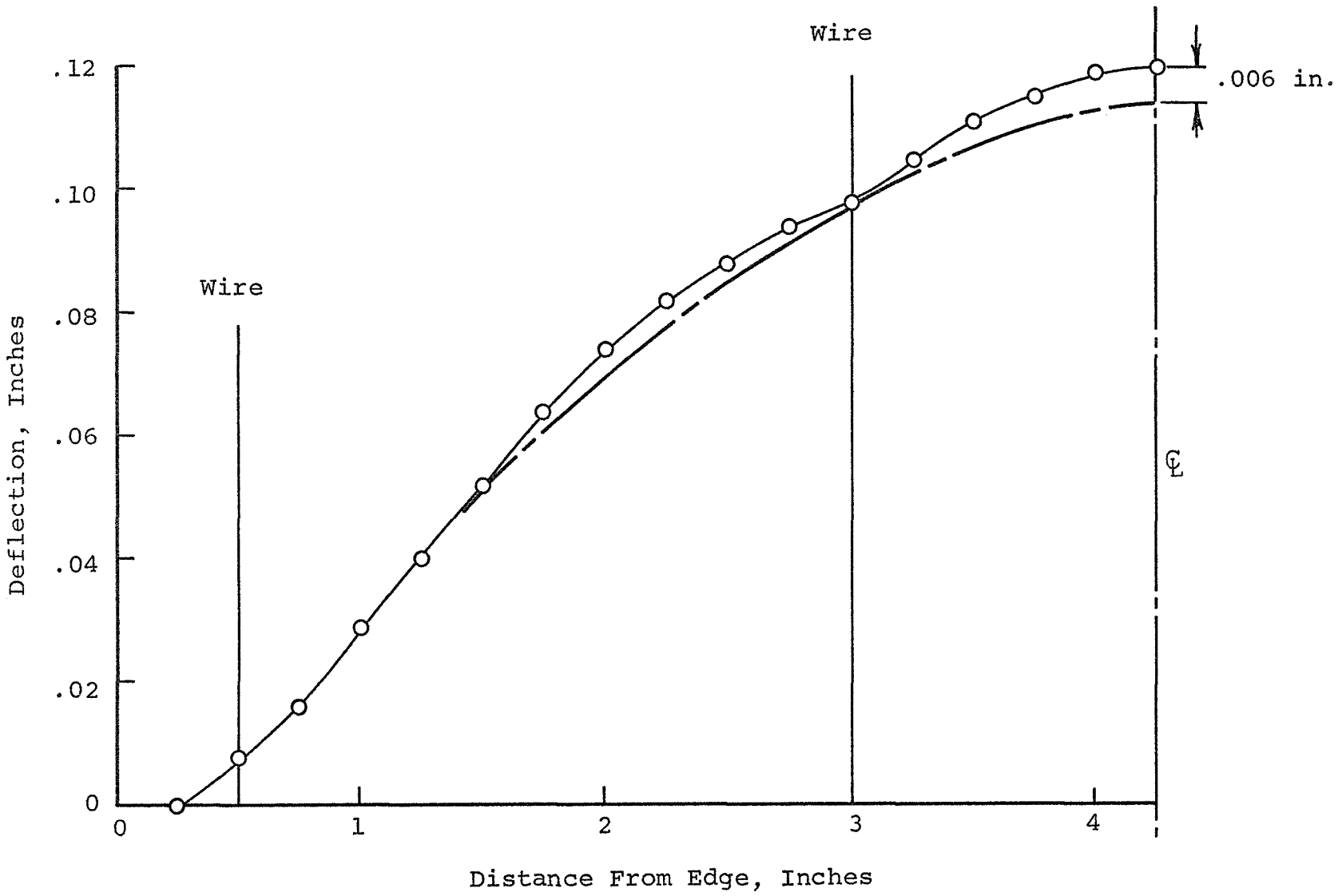

Figure 6. Deflection of Window Model, Test B

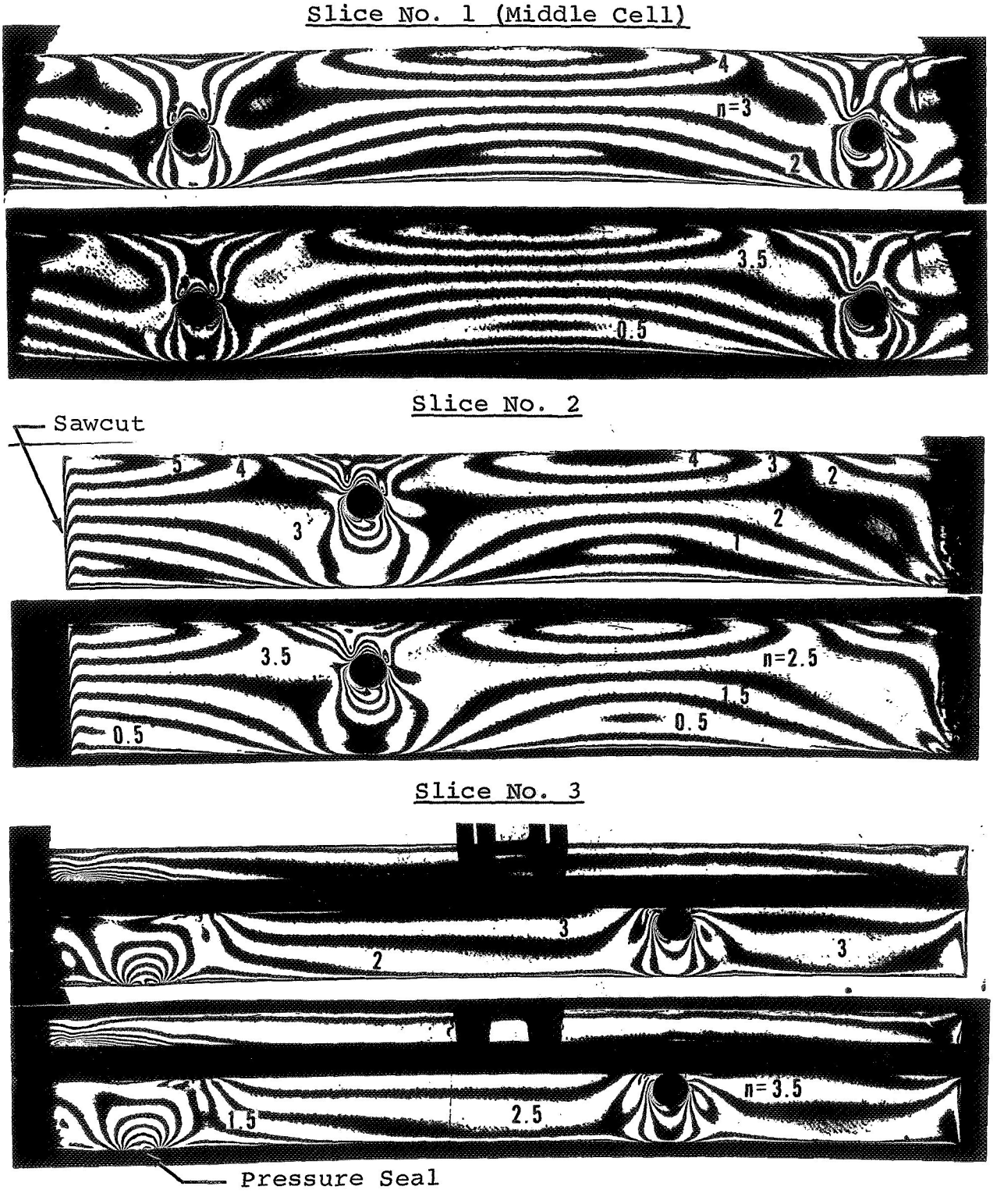

Figure 7. Frozen Stress Isochromatic Fringes, Model A
(Light Field - Top, Dark Field - Bottom)
(Numerals Denote Fringe Order)

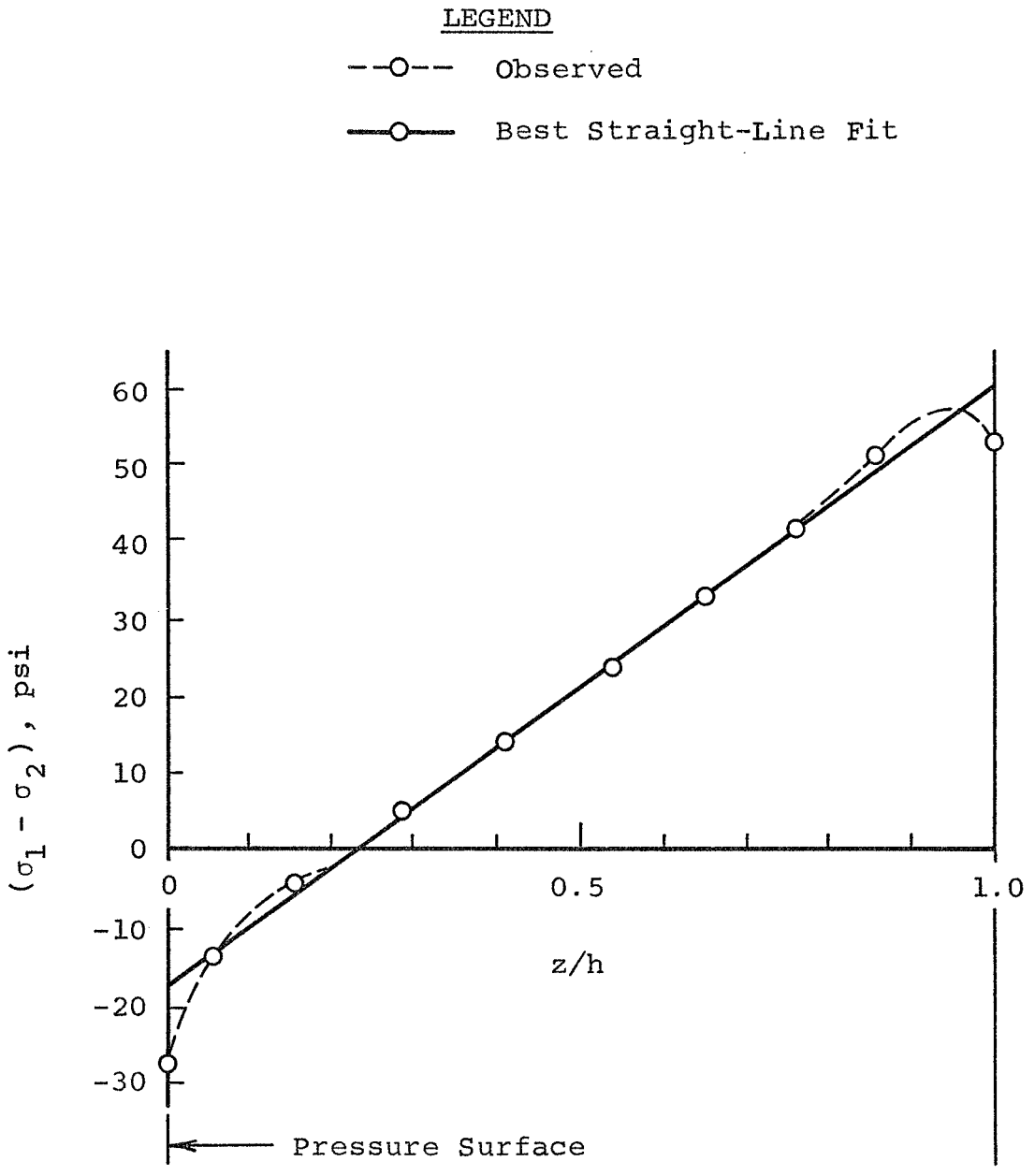

Figure 8. Stress Distribution Along Thickness at Central Point in Model A

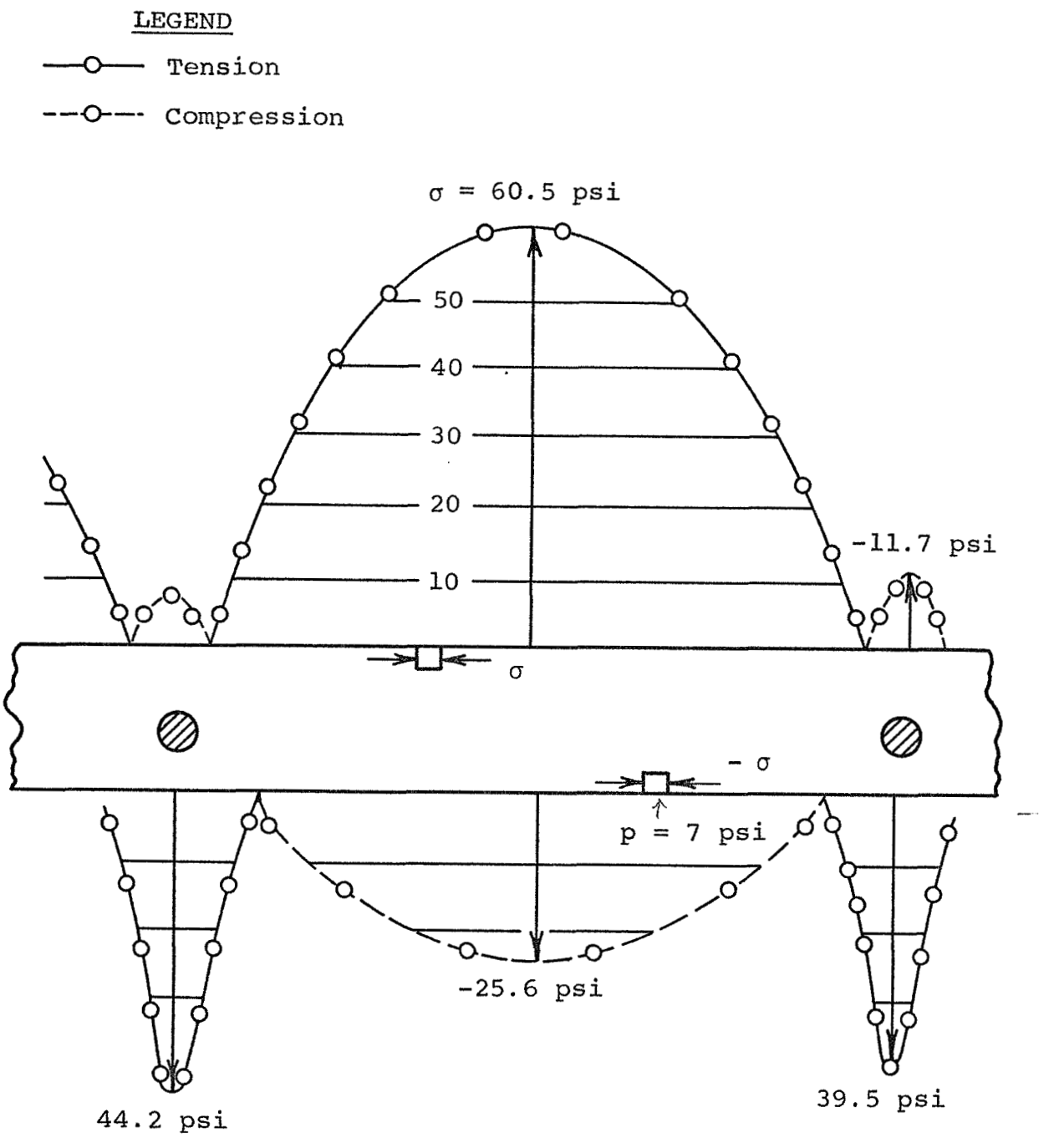

Figure 9. Boundary Stresses on Middle Cell of Slice No. 1, Model A

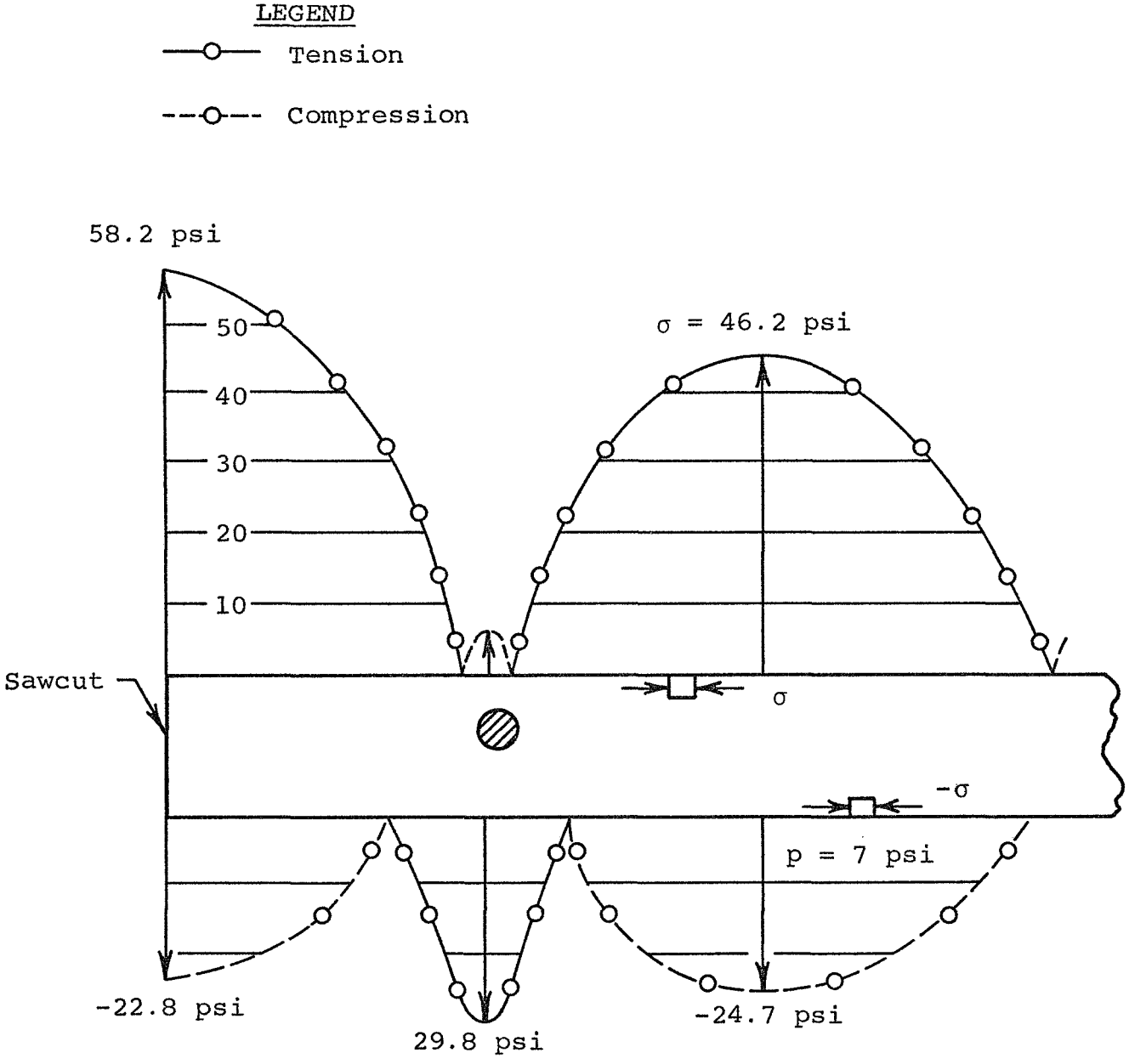

Figure 10. Boundary Stresses in Slice No. 2, Model A

Slice No. 1 (Middle Cell)

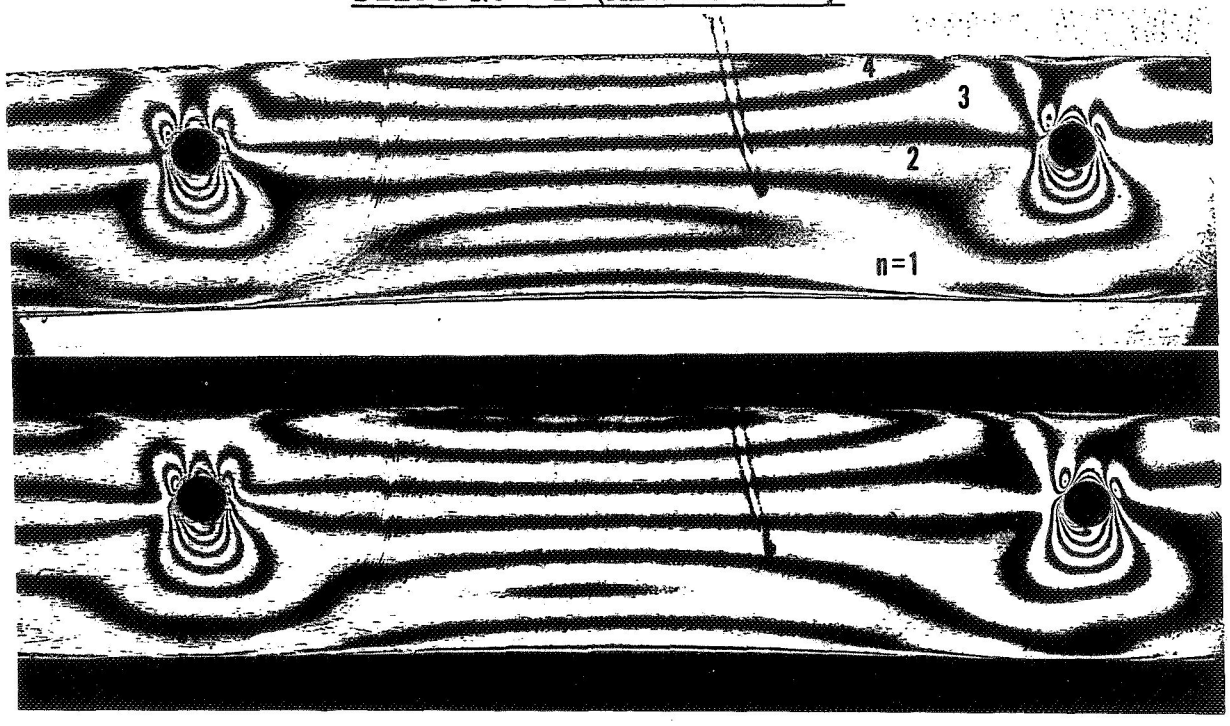

Slice No. 2

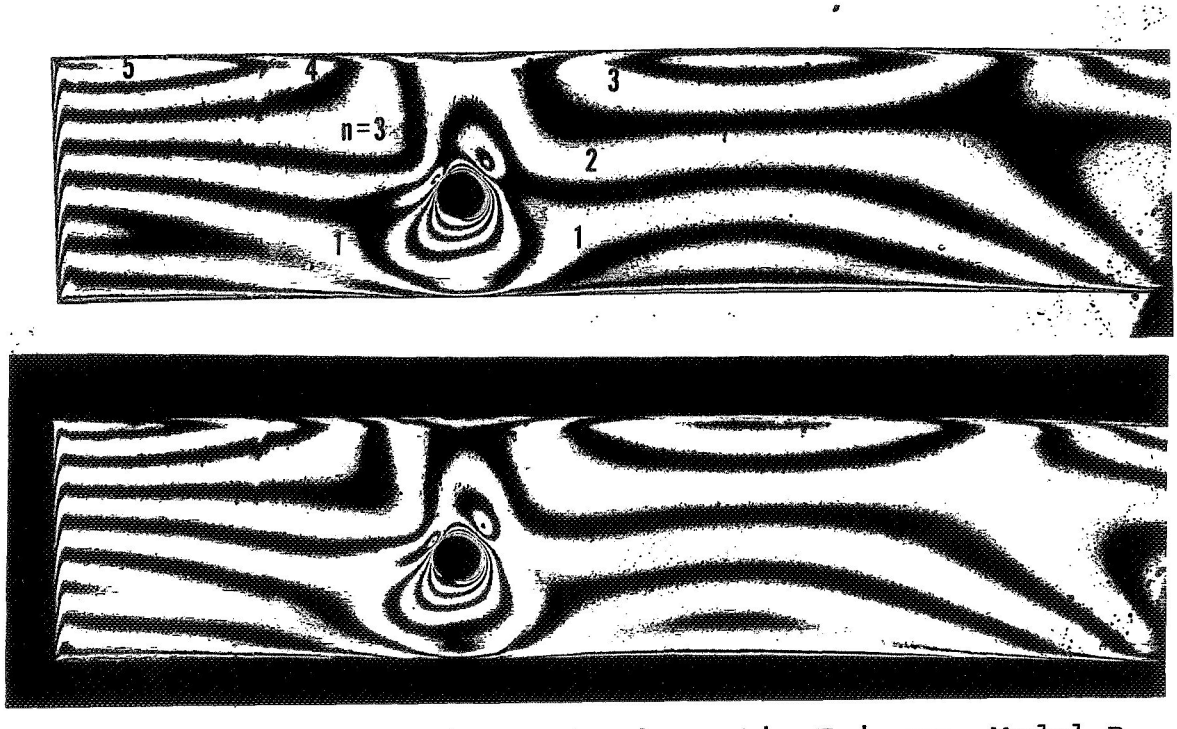

Figure 11. Frozen Stress Isochromatic Fringes, Model B (Light Field - Top, Dark Field - Bottom)

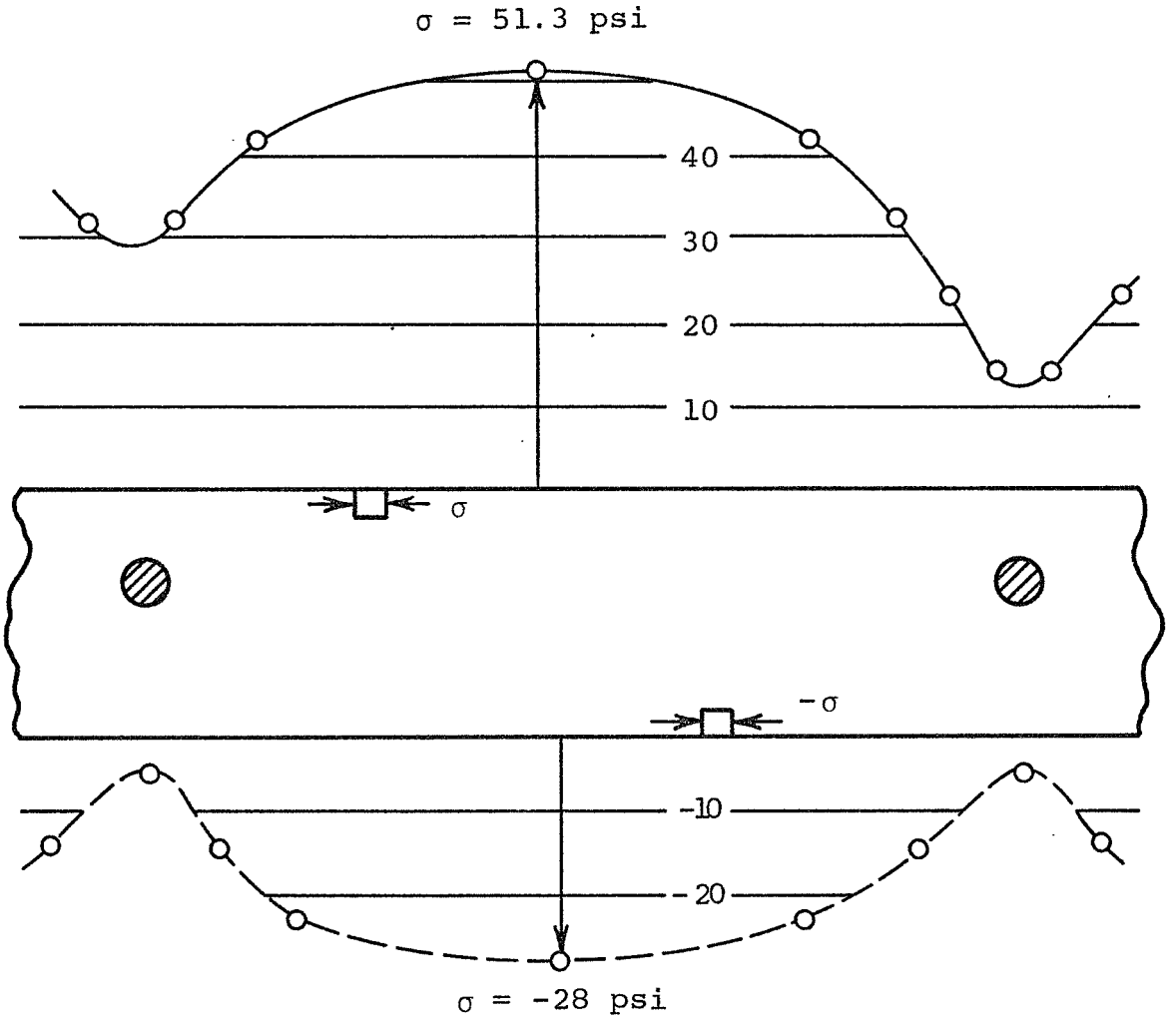

Figure 12. Boundary Stresses on Slice No. 1, Model B

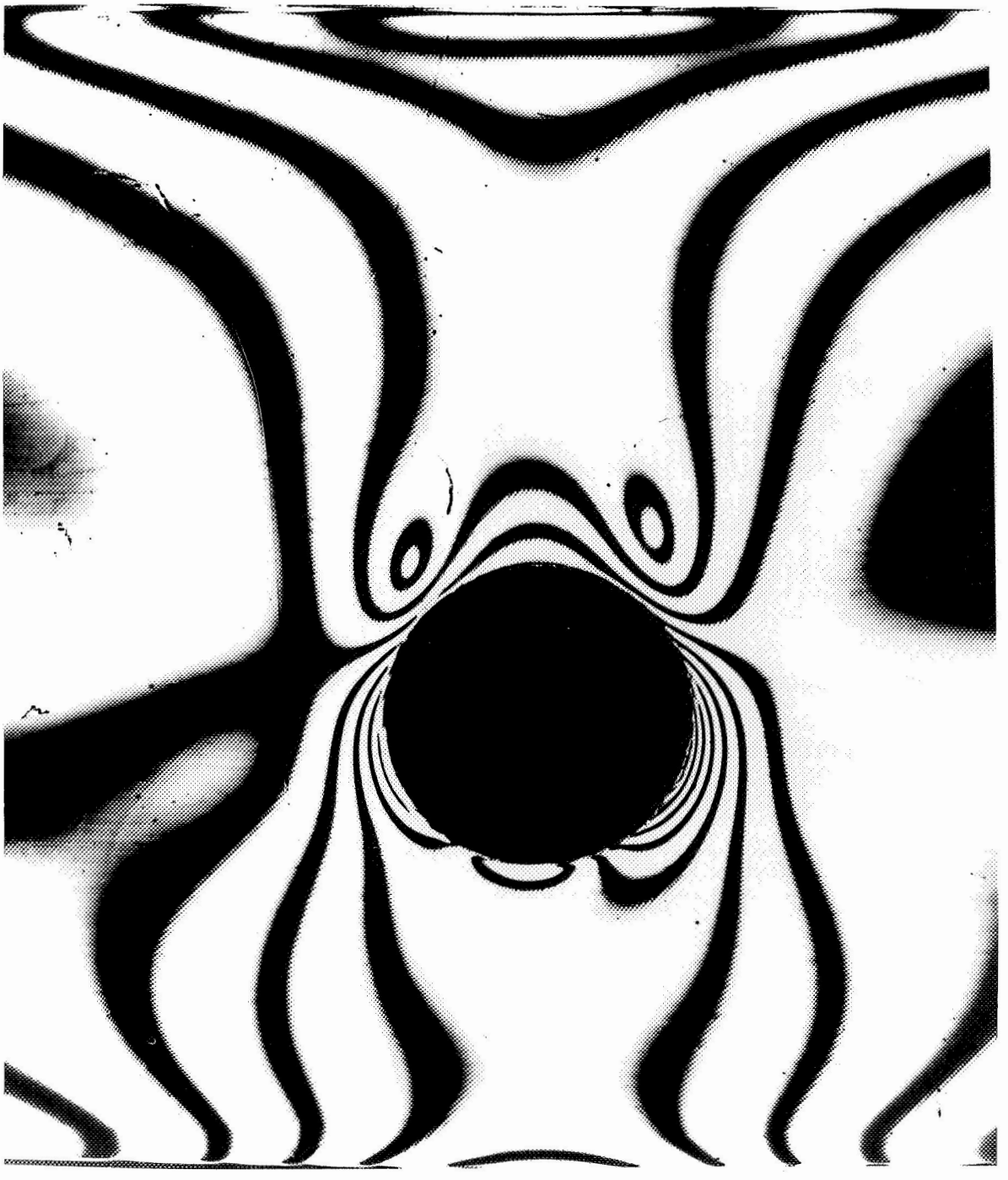

Figure 13. Isocromatic Surrounding Reinforcement Rod in Model A, Slice No. 1

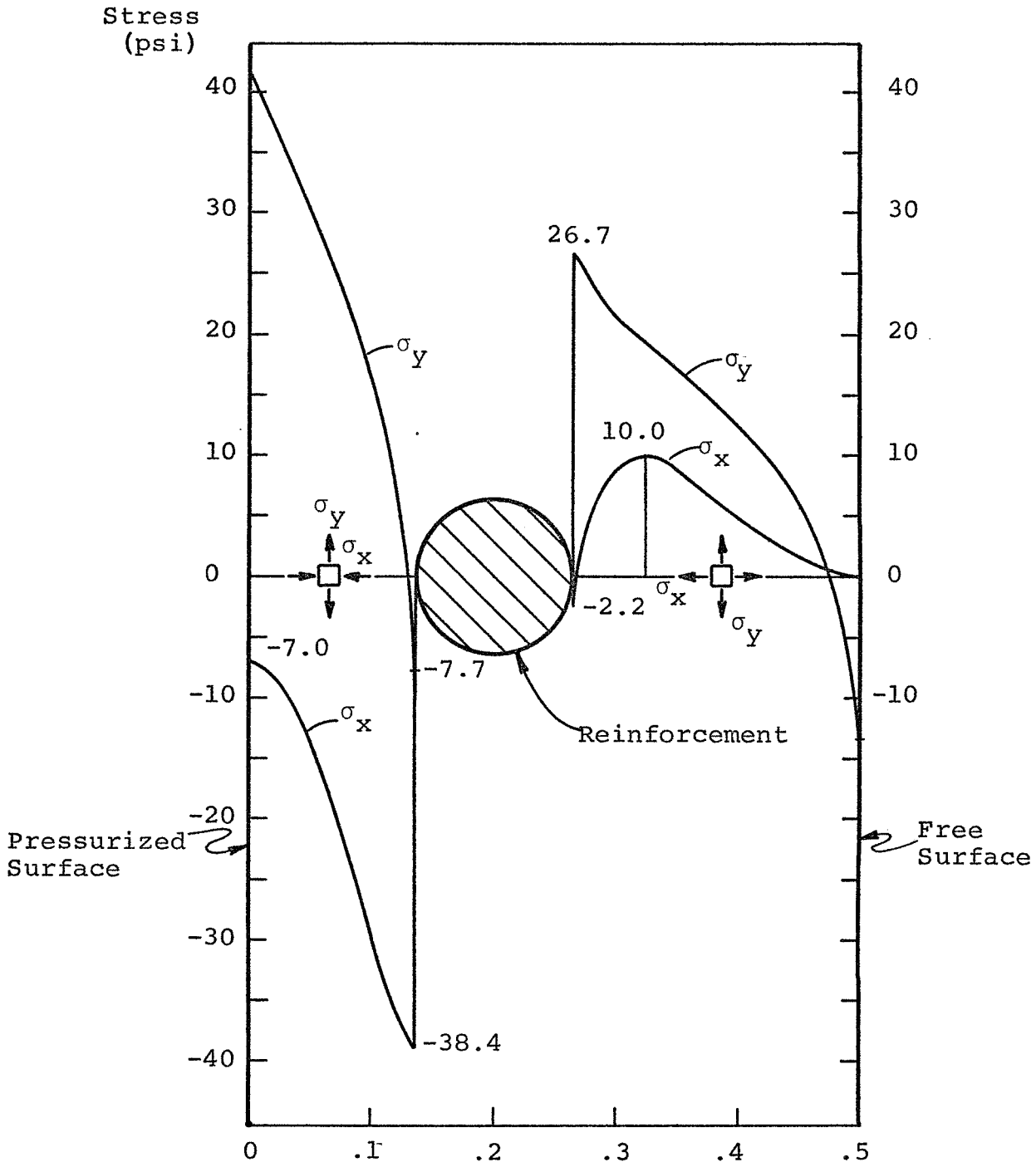

Figure 14. Stress Distribution in Slice No.1, on Section Through Reinforcing Rod

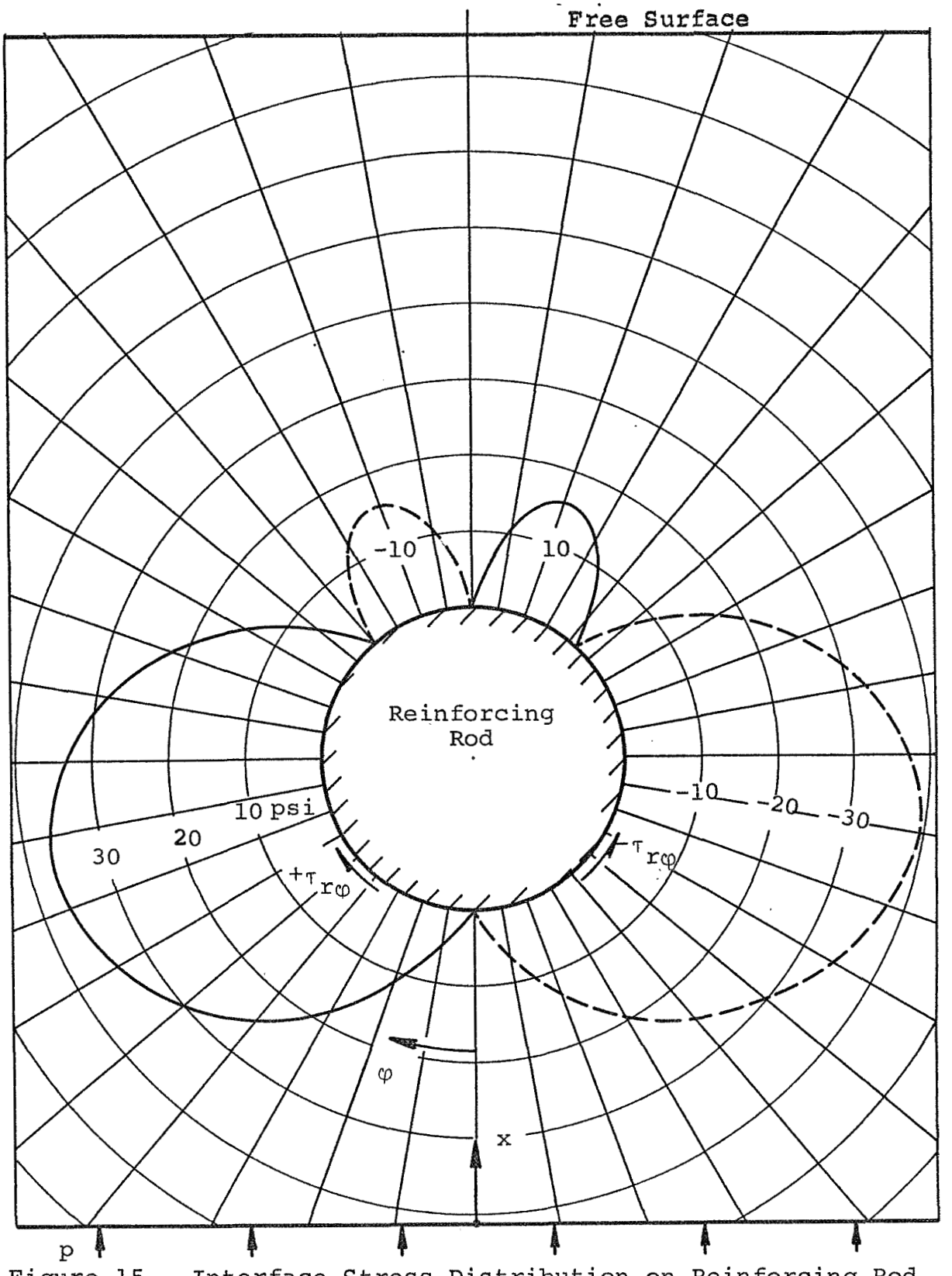

Figure 15. Interface Stress Distribution on Reinforcing Rod in Slice No. 1, Model A

REFERENCES

[1] Hille, D.E. Jr.: "Experimental and Theoretical Study for Development on an Improved Flexible Window." Uniroyal Co., Contract No. NAS 1-7771.

[2] Sampson, R.C.: "Photoelastic Studies of Solid Propellant Grain Stress Distribution." Study of Mechanical Properties of Solid Rocket Propellants, Aerojet-General Corp. Report No. 0411-10F (1962).

[3] Dally, J.W. and W.F. Riley: Experimental Stress Analysis. Chapter 10. McGraw-Hill. 1965.

[4] Sampson, R.C.: "A Three-dimensional Photoelastic Method for Analysis of Differential-Contraction Stresses." Experimental Mechanics. V. 3, No. 10. October, 1963.

[5] Timoshenko, S.: Strength of Materials, V. II. Van Nostrand. 1955-1956.

APPENDIX A

A Cursory Review of Relevant Work Reported on PHOTOELASTIC ANALYSIS OF STRESSES IN COMPOSITES

[1] Sampson, R.C.: "Photoelastic Studies of Solid Propellant Grain Stress Distribution." Study of Mechanical Properties of Solid Rocket Propellants, Aerojet-General Corp. Report No. 0411-10F (1962).

Two-dimensional square arrays of steel discs cast in place in a specially developed epoxy resin matrix were employed to determine the microstructure stress distributions in the matrix. Both thermal shrinkage and external loading conditions were evaluated separately.

[2] Sampson, R.C.: "A Three-dimensional Photoelastic Method for Analysis of Differential Contraction Stresses." Experimental Mechanics. V. 3, No. 10. October, 1963.

A general 3-D photoelastic method for photoelastic analysis of differential contraction stresses in composite structures was described. Examples were given of applications to several problems including solid rocket motors and embedded rigid inclusions.

[3] Daniel, I.M. and A.J. Durelli: "Shrinkage Stresses Around Rigid Inclusions." Experimental Mechanics. V. 2 . 1962.

Photoelastic methods were used to develop the matrix stress fringe distribution around rigid circular inclusions in shrinkage conditions.

[4] Durelli, A.J. and V.J. Parks: "New Method to Determine Restrained Shrinkage Stresses in Propellant Grain Models." Experimental Mechanics. V. 3 . November, 1963.

Two-dimensional problems of rigid inclusions in a rubber matrix were analyzed by the composite model method.

[5] Tyson, W.R. and G.J. Davies: "A Photoelastic Study of the Shear Stresses Associated with the Transfer of Stress During Fiber Reinforcement." Brit. Journal of Applied Physics. V. 16 . 1965.

The stress distribution at the interface of a rigid fiber termination in a resin matrix was determined in a field of uniaxial tension. Stress concentrations near the embedded end were evaluated.

[6] McLaughlin, T.F.: "Effect of Fiber Geometry on Stress in Fiber-reinforced Composite Materials." Experimental Mechanics. V. 6, No. 10 . 1966.

Plane stress distributions were investigated near the discontinuity of a single rigid fiber embedded in matrix. The nature and shape of the discontinuity were varied to show the effects of these parameters on the stress concentrations.

[7] McLaughlin, T.F.: "A Photoelastic Analysis of Fiber Discontinuities in Composite Materials." Journal of Composite Materials. V. 2 . 1968.

Plane arrays of parallel fibers in a photoelastic resin matrix were examined to show the effect of a discontinuity in the central one of three fibers. The nature of the eccentricity was varied so as to produce differences in the gap between fiber ends and in the eccentricity of the cut fiber ends.

[8] Pih, H. and C.E. Knight: "Photoelastic Analysis of Anisotropic Fiber Reinforced Composites." Journal of Composite Materials. V. 3 . January, 1969.

A paper similar in purpose to No. 13 but with a different approach to the solution. More extensive experimental measurements in various biaxial stress states are reported.

[9] Marloff, R.H. and I.M. Daniel: "Three-dimensional Photoelastic Analysis of a Fiber-reinforced Composite Model." Experimental Mechanics. V. 9, No. 4 . April, 1969.

Long plastic fibers in square array were cast in a matrix of epoxy resin to obtain the three-dimensional state of stress in the matrix between fibers. Both shrinkage and external loading conditions were considered and evaluated separately, following the procedures developed in Ref. (1).

[10] Stone, D.W.W.: "A Contribution to the Application of Photoelasticity to the Micromechanics of Materials." The Journal of Strain Analysis. V. 4, No. 2. April, 1969.

The author reviews some of the considerations in making photoelastic experiments of composite models.

[11] Iremonger, M.J. and W.G. Wood: "Effects of Geometry on Stresses in Discontinuous Composite Materials." The Journal of Strain Analysis. V. 4, No. 2. April, 1969.

One photoelastic solution and several finite-element numerical solutions were provided for the two-dimensional problem of a discontinuous rigid fiber reinforcing a softer matrix. Shear and normal stress concentrations near the discontinuity were obtained.

[12] Kouropoulos, T. and P.S. Theocaris: "Shrinkage Stresses in Two-Phase Materials." Journal of Composite Materials. V. 3. April, 1969.

Rigid circular disc inclusions imbedded in polymer matrices of different equilibrium modulus were examined in single and square arrays under volumetric shrinkage conditions. Stress distributions in the matrix were obtained.

[13] Sampson, R.C.: "A Stress-Optic Law for Photoelastic Analysis of Orthotropic Composites." Presented at the Fall Meeting of the Society for Experimental Stress-Analysis. October, 1969.

This paper postulates a stress-optic low for orthogonal composites in plane stress, and presents some experimental data in confirmation. It deals with the macroscopic state of stress rather than the interfiber matrix stresses that predominate on the microscopic scale.

ACKNOWLEDGMENT

This work was done at the University of Washington while the author was on leave from the Aerojet-General Corporation, Sacramento, California. These experiments were supported under NASA Grant NGR 48-002-003, under the direction of Dr. R. J. H. Bollard.